JOURNAL OF APPLIED ELECTROCHEMISTRY 27 (1997) 9–17

Fibrous metal–carbon composite structures as gas diffusion electrodes for use in alkaline electrolyte

S. AHN, B. J. TATARCHUK

Department of Chemical Engineering and the Space Power Institute, Auburn University, AL 36849, USA

Received 13 September 1996; revised 26 February 1996

The fabrication of novel fibre composite electrode structures and the performance assessments for oxygen reduction in alkaline electrolyte is reported. An array of 2μm diameter activated carbon fibres interlocked within a network of 2μm sinter-bonded metal fibres to form the composite structure was used. The resulting electrode structure is stable, highly conductive and can maintain void fraction exceeding 95%. Electrode physical properties including thickness, macroporosity, volume and mass fractions of constituent carbon and metal fibres have been controlled, characterized, and related to the electrode polarization in a KOH half cell. Comparisons have been made with a commercial Teflon-bonded gas diffusion electrode (GDE). It has been demonstrated that this novel method allows reproducible and low-cost fabrication of GDEs with the optimal balance between macropores for gas access, micropores for liquid access, and conductive paths for electron access.

1. Introduction

Carbon-based electrodes are currently used in a number of electrochemical energy conversion devices, including fuel cells and batteries [1–3]. The maximum energy and/or power densities obtainable from these electrodes depend on various physicochemical rate phenomena occurring at the electrode–electrolyte interface.

In the case of fuel cells and other electrocatalytic processes, the power levels depend on heat and mass transport rates, conduction of electrons and ions in the electrode, and charge transfer rates across the interface [4]. Devices with higher power levels require new types of electrode structures that can increase appropriate reaction/transport rates within the 'three-phase interfacial zones' occurring between: (i) the gaseous reactants (e.g., O_2, H_2), (ii) the electrolyte (e.g., KOH, H_3PO_4, ion-conducting membrane), and (iii) the electrocatalyst (e.g., Pt/carbon). Also, the choice of appropriate electrode structures and materials depends on: (i) corrosion issues in acidic versus alkaline media, (ii) needs for electrocatalysts in anodes and cathodes, (iii) cost versus applications, and (iv) other critical factors such as sintering of catalysts and overall device lifetimes.

In conventional electrode structures, carbon blacks are often utilized in a particulate form and hot-pressed onto a collector screen using polytetrafluoroethylene (PTFE) and/or other types of thermoplastic/organic binders [5]. The PTFE binder is also employed to provide a network of gas channels within the electrode structure.

The approach chosen here is to utilize high aspect ratio carbon fibres and conductive metal fibres to form a highly porous yet physically stable composite structure. Unlike conventional electrode structures utilizing particulate-based carbons and binders; use of high aspect ratio fibres permits fabrication of self-supporting electrodes from 20% to $\geqslant 98\%$ void volume. Moreover, the architecture of the metal-fibre carbon-fibre composite electrode permits variation in surface area, microporosity, macroporosity, void volume, electrocatalyst loading, and electrode thickness in regimes not permitted by packed-particulate systems. As such, this electrode structure provides an ideal opportunity to probe various intraelectrode processes in a relatively straightforward and independent fashion.

A procedure was recently developed in this laboratory [6–10] for combining high surface area carbon fibres (ca. 2μm diameter) and 2μm diameter stainless steel fibres into a composite electrode structure comprising a stable nonwoven network of carbon fibre trapped within a network of sinter-bonded metal fibres. The resultant high surface area-high conductivity composite was anticipated to allow high accessibility to gases and electrolytes while providing adjustable porosities and void volumes. The electrodes thus prepared were characterized and optimized for specific applications in a liquid double-layer capacitor [7].

The goal of this study was to develop structures with properties well-suited for air electrode applications. Fibrous carbon-stainless steel composite electrodes were fabricated for use as cathodes in KOH half cells. Stainless steel fibres were chosen because of their commercial availability in small diameters ($\leqslant 4\,\mu$m) and their compatibility with alkaline electrolytes. Efforts were focused on the oxygen reduction reaction, which is known to control the overall reaction in H_2–O_2 fuel cells [11], zinc/air batteries [12], iron/air cells [13], lithium/air, and aluminium/air batteries [2]. Electrodes with different structural characteristics and compositions were fabricated to examine the effects of various loadings of carbon,

0021-891X

metal, binders and pore formers. The performances of the composite electrodes were assessed during oxygen reduction in KOH half-cells. The polarization curves from composite electrodes were also compared to those determined from a commercial powder-based Teflon-bonded fuel cell electrode.

2. Experimental details

2.1. *Electrode preparation*

The constituent materials employed during electrode preparation were: carbon fibres (Charcoal Cloth, Limited), 316L stainless steel fibres (Memtec), and cellulose fibres (a mixture of soft and hard woods). Individual carbon fibres were 2 to 3 μm in diameter but were used as 20 μm diameter bundles containing about 30 individual fibres. Bundles were up to 5 mm in length and the specific BET surface areas were about 750 $m^2 g^{-1}$ with a mean pore radius of 3 nm. The BET area and pore size distribution were determined from nitrogen adsorption and desorption isotherms at 77 K, respectively. The stainless steel fibres were $\leqslant 4$ μm in diameter and 2 mm in length. Cellulose fibres were 20 to 30 μm in diameter and varied in length from 100 to 1000 μm.

Carbon–stainless steel–cellulose composite papers (i.e., paper preforms) were prepared as 16 cm diameter circular sheets (200 cm^2 geometric area) in a conventional paper making apparatus as outlined previously [6, 8]. Paper preforms with different loadings of carbon fibres, stainless steel fibres, and cellulose fibres were prepared (see Table 1). Stainless steel-cellulose composite papers containing 2.5 mg cellulose per cm^2 and 2.5 mg stainless steel per cm^2 were also prepared for use as protective overlayers and as current collectors (see Fig. 1). The sandwiching metal overlayers

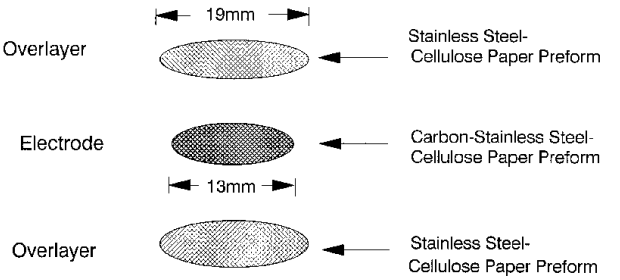

Fig. 1. Fabrication of electrode; stacking of paper preforms into an electrode preform prior to sintering.

provided a structural reinforcement to carbon containing active layers and kept the carbon fibres at the top layer entrapped within the electrode structure.

Paper preforms were cut and layered as shown in Fig. 1. The preforms were pressed at ~100 MPa before sintering. The electrode preforms were then sintered as described in detail in previous investigations [6, 7]. Sintering was performed at 1323 K for 30 min in an atmosphere of pure hydrogen (99.995%, liquid air) within a 3.2 cm i.d. quartz tube at a linear flow rate of 2.6 cm min^{-1} (STP) at a total pressure of 101 kPa. Finished electrodes were pressed onto porous Teflon films (Tetratec Corporation). The Teflon films were approximately 25 μm thick, 80 to 90 vol% porous, and provided an equivalent pore size of ~0.22 μm.

2.2. *Electrochemical cell*

Experiments were carried out in a transparent plastic half-cell (Quickcell™, Electrosynthesis, Inc., Fig. 2). The working electrode was placed between two polyethylene gaskets with the counterelectrode (platinum disc, Johnson Matthey) mounted at the opposite side of the cell. The active geometric area of both electrodes was 1.33 cm^2. Feed gas (O_2, 99.5%) at an

Table 1. Physical properties of the electrodes tested in this study

Electrode	*Preform composition* [*C*/*SS*/*cell*] /g $sheet^{-1}$	*Composition after sintering* [*C*/*SS*] /mg cm^{-2}	*Carbon retention after sintering* /%	*Electrode thickness* /mm	*Volume fraction* [*C*/*SS*]	*Macroporosity*
C1	0.1/1.0/0.5	0.4/5.0	86	0.04	0.10/0.16	0.75
C2	0.5/1.0/0.5	2.0/5.0	82	0.08	0.24/0.08	0.68
C3	1.0/1.0/0.5	3.5/5.0	71	0.14	0.24/0.05	0.71
C3PT‡	1.1/1.0/0.5	3.4/5.1	62	0.13	0.25/0.05	0.70
L1	1.0/1.0/0.1	3.8/5.2	72	0.15	0.24/0.04	0.72
L2	1.0/1.0/0.5	3.2/4.9	66	0.14	0.21/0.04	0.75
L2NP†	same as L2	3.4/4.9	69	0.30	0.11/0.02	0.87
L3	1.0/1.0/1.0	3.8/5.3	72	0.15	0.24/0.04	0.71
L3NP†	same as L3	3.5/5.1	68	0.40	0.08/0.02	0.90
*S1	1.0/0.1/0.5	4.4/0.5	93	0.16	0.26/0.04	0.74
*S2	1.0/0.5/0.5	5.0/2.6	97	0.17	0.28/0.02	0.70
*S3	1.0/1.0/0.5	3.7/4.9	75	0.16	0.22/0.04	0.74
*2S1	two layers of S1	8.2/0.9	91	0.22	0.35/0.01	0.64
*3S1	three layers of S1	11.1/1.4	82	0.29	0.36/0.01	0.63

[C/SS/Cell] ≡ carbon/stainless steel/cellulose, sheet is 16 cm diam. (200 cm^2 geometric area).
* With 4 μm diameter stainless steel fibres instead of nominal 2 μm.
† NP Not mechanically pressed, all others pressed at ~100 MPa.
‡ PT With platinum-impregnated carbon fibres.

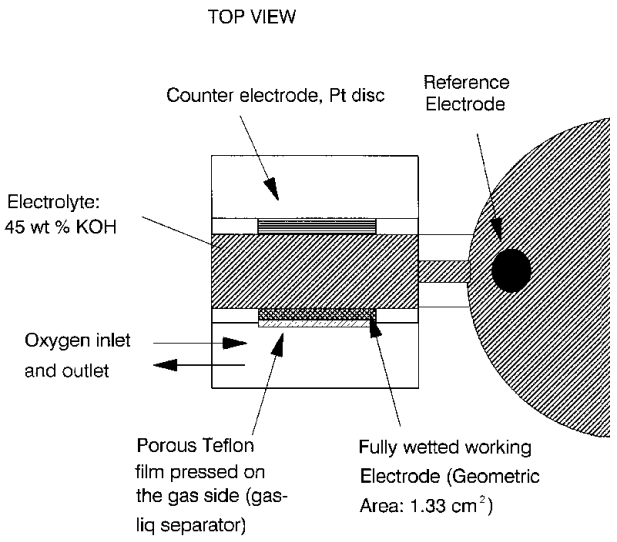

Fig. 2. Schematic of test cell.

overpressure of ~0.4 kPa was supplied to the gas chamber on the back side of the test electrode. The electrolytic solutions (45 wt % KOH, Fisher Scientific) was circulated through the electrolyte chamber and toward the reference electrode using a gas lift pump. A small hole in the electrolyte chamber near the test electrode served as a connection to the reference electrode compartment. A saturated calomel electrode (Fisher Scientific) was used as a reference. The reference electrode was checked frequently between experiments against a freshly filled reference of the same type to ensure accurate overpotential measurements. All experiments were conducted at room temperature.

2.3. *Electron microscopy*

Scanning electron microscopy (SEM) was utilized to observe structural characteristics of the electrodes. Micrographs were prepared on an ISI model 5540 scanning electron microscope at 5 kV beam energy.

2.4. *Polarization measurements*

Electrodes were spot-welded to 0.25 mm diameter nickel wires (99.995%, Johnson Matthey). Electrochemical measurements were made using an EG&G Princeton Applied Research System including an EG&G PARC model 273 potentiostat/galvanostat, and an IBM model 30 microcomputer. Galvanostatic and potentiostatic measurements were employed to obtain cell potential against current. In potentiostatic measurements, the electrode potentials were swept from the open circuit potential to lower potentials at a scan rate of 1 mV s^{-1}.

3. Results and discussion

3.1. *Effects of preparation variables*

Electrode physical properties including thickness, macroporosity, volume fractions of carbon and metal fibres, and compositions before and after sintering are summarized in Table 1. The amount of carbon retained in the electrode after sintering was determined from weight change measurements and earlier observations indicating that cellulose was almost totally removed during sintering [7]. Electrode thickness was measured using a micrometer. Each electrode was held between two flat quartz plates to prevent pressing and deforming by the micrometer tips. The volume fractions of carbon and metal fibres and the macroporosity were calculated from fibre loadings, fibre densities and electrode thickness.

Table 2. Electrode kinetic parameters obtained by fitting polarization data with equation $E = E_0 - b \log i - iR$, *where* $E_0 = E_r + b \log i_0$

Electrode	E_0/mV vs SCE	E_r	$10^4 i_0^a$/A cm^{-2}	b/mV dec^{-1}	R/Ω cm^2	R_e/Ω cm^2
L1	−303	−268	1.4	40.4	1.17	0.75
L2	−288	−274	4.7	43.0	1.29	0.75
L2NP†	−307	−268	1.1	40.0	1.74	0.74
L3	−290	−273	3.8	40.9	1.27	0.74
L3NP†	−268	−255	5.0	43.4	4.83	0.77
C1	–	−363	–	–	–	0.76
C2	−309	−280	2.0	41.4	1.41	0.74
C3	−295	−272	2.7	40.5	1.17	0.74
C3PT‡	−225	−214	5.4	41.3	1.20	0.75
*S1	−303	−259	0.8	40.0	1.38	0.75
*2S1	−295	−262	1.7	42.5	1.43	0.75
*3S1	−282	−256	3.0	50.3	1.52	0.77
*S2	−278	−249	2.6	50.2	1.15	0.76
[b] $n = 1$ hi p	−270	−267	8.6	44.2	0.87	0.76
[b] $n = 3$	−279	−275	7.9	40.0	1.25	0.75
[b] $n = 9$	−264	−263	9.4	40.0	1.69	0.74
Prototech	−207	−110	0.04	40.0	1.74	0.98

* With 4 μm diam. stainless steel fibres instead of nominal 2 μm.
† NP Not mechanically pressed, all others pressed at ~100 MPa.
‡ PT With platinum-impregnated carbon fibres.
[a] i_0 is calculated using equation $E_0 = E_r + b \log i_0$.
[b] n represents the number of stainless steel overlayers placed at the gas side of C3 composite electrode. hi p denotes operation at higher oxygen pressure (0.93 kPa). See Fig. 11.

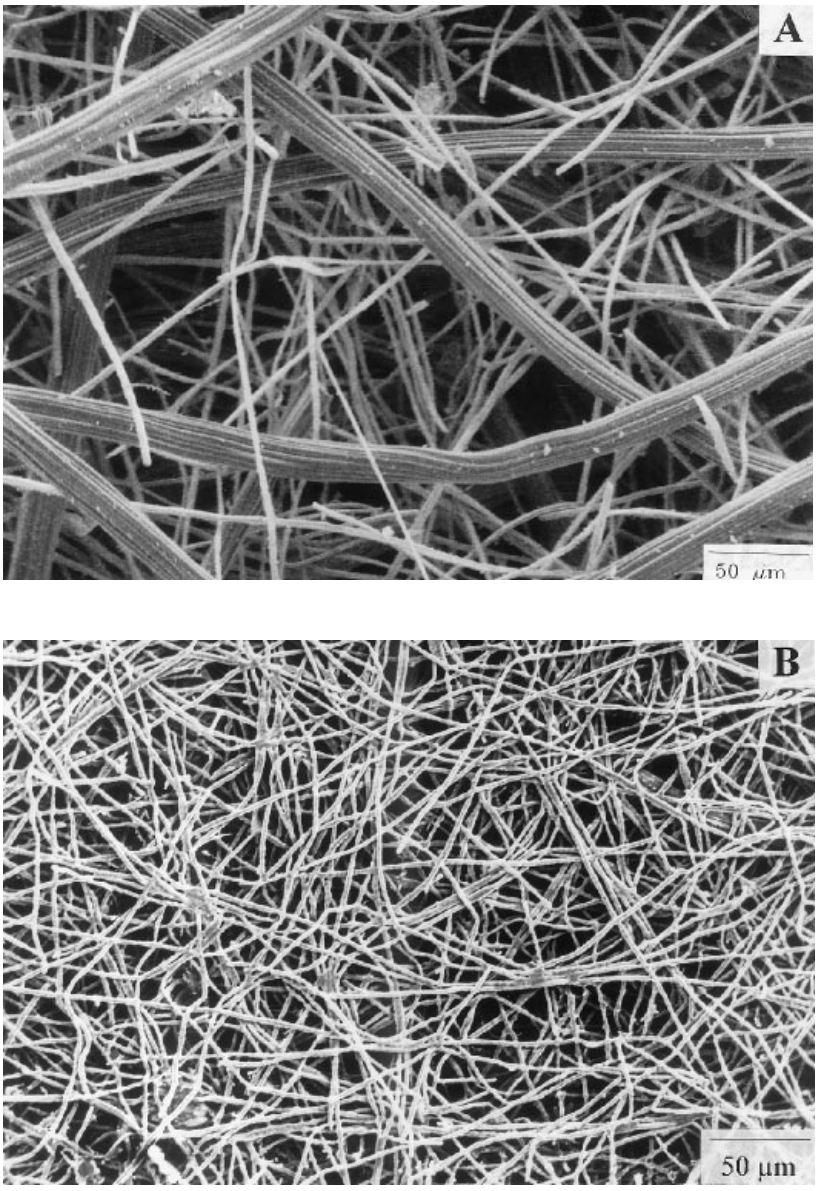

Fig. 3. (a) SEM micrograph of the unpressed electrode (L2NP, Table 1). Electrode sintered at 1323 K for 30 min. Carbon loading: 3.4 mg cm^{-2}. Stainless steel loading: 4.9 mg cm^{-2}. Note: stainless steel fibres are 2μm diam. (b) Stainless steel mesh overlayer (i.e., exterior of electrode sandwich). Sintered at 1323 K for 30 min. Metal loading: 2.5 mg cm^{-2}.

3.2. *Evaluation of electrode kinetic, ohmic and mass transport parameters from polarization data*

The half cell potential, E, against current density, i, data were analysed using the equation [16, 17]:

$$E = E_0 - b \log i - iR \quad (1)$$

where

$$E_0 = E_r + b \log i_0 \quad (2)$$

In these equations, E_r is the reversible potential for the electrode, b and i_0 are the Tafel slope and exchange current density for the oxygen reduction reaction, respectively. R represents the resistance, which causes a linear decrease of the electrode potential with current density. The contributions to R are from extra- and intra-electrode ohmic resistances and from mass transport resistance, which is apparently constant over limited current density range [17], but then increases rapidly leading to a limiting current.

The parameters E_0, b and R were evaluated by nonlinear least squares fitting of the experimental data to Equation 1. The data points beyond the end of linear region of E against i were excluded in the regression. The results are summarized in Table 2 and will be discussed in the following Sections.

The tested composite electrodes exhibited Tafel slopes ranging from 40 to 50 mV dec^{-1} and external ohmic resistances of $0.75 \pm 0.01\,\Omega\,\text{cm}^2$, which were measured via a.c. impedance spectroscopy [15]. The external ohmic resistance, R_e, represents the uncompensated solution resistance, the contact resistance between the electrolyte and electrode, and the electronic resistances of lead wires and electrical contacts.

3.3. *Effect of preform pressing*

The thickness of the sintered electrodes, L2NP and L2, decreased from 0.30 to 0.14 mm as a result of mechanical pressing of the electrode preform prior to sintering. As observed from the SEM micrographs

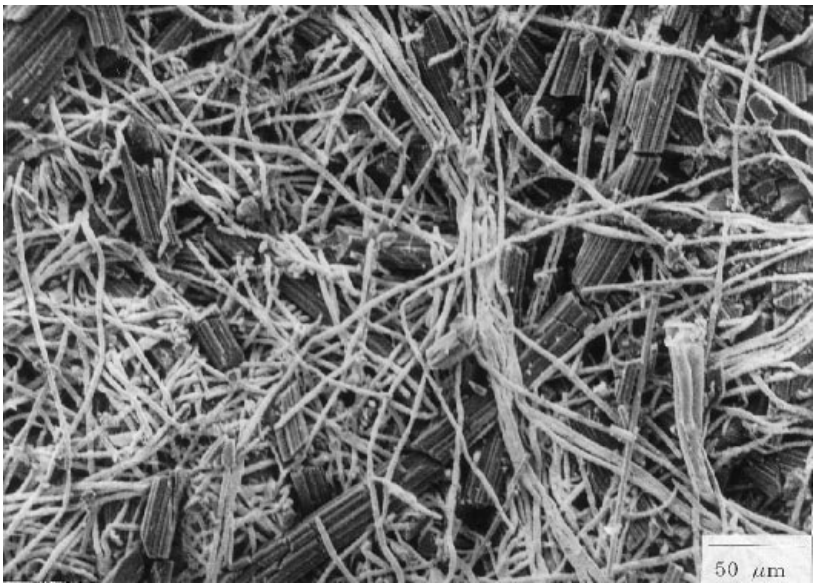

Fig. 4. SEM micrograph of the pressed electrode (L2, Table 1) prepared at 100 MPa. Electrode sintered at 1323 K for 30 min. Carbon loading: 3.2 mg cm^{-2}. Stainless steel loading: 4.9 mg cm^{-2}. Note: stainless steel fibres are 2μm diam.

shown in Figs 3 and 4, mechanically pressing the preforms yields a more compact structure with less void space between fibres. Polarization curves typically expected for pressed and unpressed electrodes (namely, L2 and L2NP, Table 1) are shown in Fig. 5. The limiting current density was fairly low ($\sim$30 mA cm^{-2}) for the unpressed electrode while no current limitation was observed for the pressed one upto about 250 mA cm^{-2}. The open structure of the unpressed electrode places less of its active catalytic carbon material in close proximity to the gas plenum where the concentration of dissolved oxygen gas within the electrolyte is high. Therefore, oxygen must diffuse via a longer pathway to reach active sites. The *R* values in Table 2 confirm this situation and are higher for the unpressed electrodes (L2 against L2NP and L3NP).

3.4. *Effect of carbon loading*

Electrodes with different levels of carbon were prepared using paper preforms containing 0.5, 2.5 and 5.0 mg of carbon cm^{-2} while maintaining constant cellulose (2.5 mg cm^{-2}) and stainless steel loadings (5.0 mg cm^{-2}). Figure 6 is a plot of potential against current density for different carbon loadings (electrodes C1, C2 and C3 in Table 1). A blank electrode was also fabricated using two stainless steel–cellulose overlayers with no active metal–carbon layer between these overlayers. As the carbon loading increased from zero to 3.5 mg cm^{-2}, the polarization curves became more flat as expected, due to increased activity by the carbon catalyst.

As shown in Fig. 6, the electrode with 2.0 mg carbon cm^{-2} (viz. C2) quickly reached its limiting current density compared to the electrode with 3.5 mg cm^{-2}. For electrode C2, with a reduced number of carbon fibres within the critical gas–liquid reaction zone, the reaction was forced to occur further within the interior of the microporous carbon fibres at higher overpotentials. In the interior the effective diffusivity is lower, resulting in the onset of severe intraparticle mass transport limitations and reduced current densities. The reaction

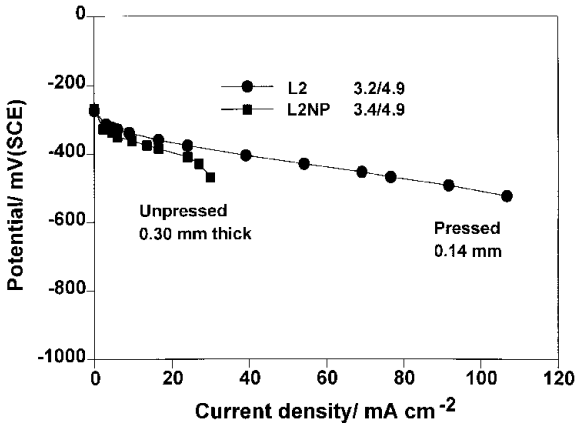

Fig. 5. Electrode polarization: effect of mechanically pressing preform sheet prior to sintering. The unpressed and pressed electrodes are L2NP (■) and L2 (●) with their respective composition after sintering given in Table 1.

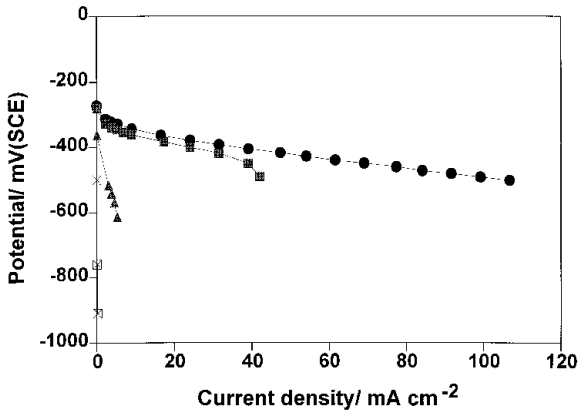

Fig. 6. Effect of carbon fibre loading on electrode polarization. Stainless steel loadings were constant (5.0 mg cm^{-2}). Blank electrode (☒) is composed of stainless steel overlayers only. Key: (●) C3, (■) C2, (▲) C1, with respective compositions after sintering given in Table 1.

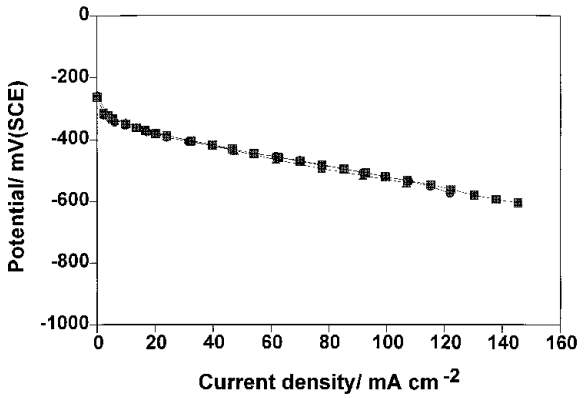

Fig. 7. Effect of preform stacking on electrode polarization. Key: (●) S1, (■) 2S1, (▲) 3S1 with respective compositions after sintering given in Table 1.

was also noted to be most facile at the exterior of the carbon fibre.

Since the data in Fig. 6 indicate that enhanced electrode performance is obtained by increasing the carbon (catalyst) loading, the effect of carbon loadings above 3.5 mg cm^{-2} was also examined. Increased carbon loadings were achieved by placing two and three active carbon–metal composite sheets between the stainless steel overlayers. In these electrodes (S1, 2S1 and 3S1, Table 1) the stainless steel loading increased in proportion to the number of sheets utilized. Polarization curves in Fig. 7 show that having two or more active layers did not bring a notable enhancement in the electrode performance within the current density region examined, indicating only a small portion of the electrode closest to the gas side was being utilized in the reaction. The electrode parameters in Table 2 suggest that electrode activities, indicated by E_0 values, are marginally higher for the multiply layered electrodes. The R values are also larger with the thicker electrodes, possibly due to increased intraelectrode ohmic resistances [15].

3.5. *Effect of stainless steel loading*

Polarization curves for electrodes S1, S2, and C3, in Table 1, were obtained from preforms with varying stainless steel loadings but with constant levels of carbon and cellulose (Fig. 8). The linear resistance, R, was observed to decrease from 1.38 to 1.15 Ω cm^2 when the metal loading was increased from 0.5 to 2.6 mg cm^{-2}. This decrease can be attributed to the reduction in the intraelectrode ohmic resistance, as evidenced by a separate a.c. impedance measurement [15]. The increase in metal loading appears to provide an increased number of sintered metal joints and metal–carbon contacts. However, the R value remained approximately constant when the metal loading was increased from 2.6 to 5.0 mg cm^{-2} because the electrical resistance of the electrode with 2.6 mg metal cm^{-2} was already near its minimum value.

3.6. *Effect of cellulose loading in the preform*

In the preform, cellulose acts as both a binder [6] and a void former. Thus, the macroporosity observed after sintering depends, to some degree along with mechanical pressing, on the amount of cellulose used in the preform. For unpressed electrode preforms, the sintered electrode thickness and macroporosity increase with cellulose loading (see L2NP and L3NP in Table 1). Figure 9 shows the polarization curves for electrodes L1, L2, L3 and L3NP as obtained from preforms with varying amounts of cellulose but with fixed levels of both carbon and stainless steel. The unpressed electrode with highest cellulose loading (L3NP) exhibited highest R due to increased mass transport resistance and internal ohmic resistance caused by loose contacting between fibres. However, Fig. 9 also shows that electrodes L1, L2 and L3, prepared by mechanical pressing before sintering, are apparently sufficiently thin that the effect of cellulose on electrode performance was not pronounced.

3.7. *Critical thickness in the composite electrode*

According to the above results, the most significant factors affecting electrode polarization are carbon loading and electrode pressing. The electrode performance increased significantly until carbon loading reached a value of about 3.5 mg cm^{-2} and exhibited no further improvements for higher loadings. When

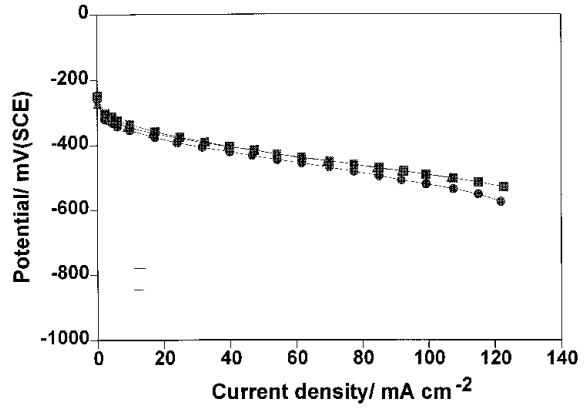

Fig. 8. Effect of metal fibre loading on electrode polarization. Key: (●) S1, (■) S2, (▲) C3 with respective compositions after sintering given in Table 1.

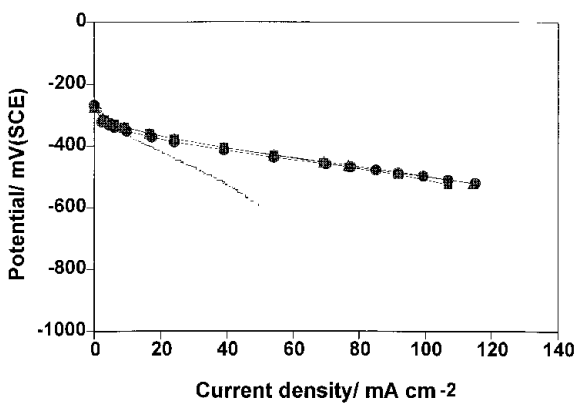

Fig. 9. Effect of cellulose fibre loading in paper preform on electrode polarization. [C/SS/Cell]/mg cm^{-2}: (●, L1) 3.8/5.2/0.5; (■, L2) 3.2/4.9/2.5; (▲, L3) 3.8/5.3/5.0; (—, L3NP) 3.5/5.1/5.0.

the electrode was not pressed prior to sintering, the thickness increased considerably. The thicker unpressed electrodes with comparable levels of carbon showed lower performance.

The above observations suggest that there exists a 'critical thickness' within the composite electrode where gas–liquid transport is facile and catalyst loading and activity must be optimized. The critical reaction zone is visualized in Fig. 10. Electrode pressing can be used to concentrate carbon within this thickness, increasing the utilization of carbon. The addition of carbon was effective in enhancing the performance only within this thickness regime.

To verify this controlling diffusion and reaction processes, the location of this critical thickness region was displaced from the Teflon separator by placing more inert stainless steel overlayers at the gas side of the electrode. The drawing in Fig. 11 depicts the composite electrodes with different number of overlayers. As shown in Fig. 11, the electrode with three overlayers provided a lower limiting current density ($\sim 75\,mA\,cm^{-2}$) than the electrode with only one inert stainless steel overlayer between the Teflon separator and the carbon/stainless steel active layer. The limiting current density was further reduced when nine overlayers were placed at the gas side of the electrode. It is interesting to note that performance in the lower current density region was slightly higher for electrodes with more stainless steel overlayers. The excess amount of stainless steel at the gas–liquid interface may have contributed to enhancing kinetics itself and/or by contacting more

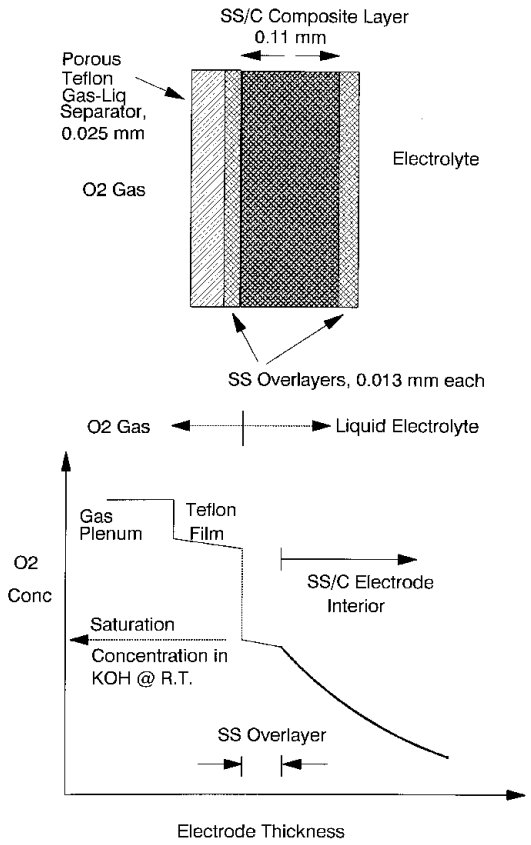

Fig. 10. Composite electrode model showing the critical thickness region.

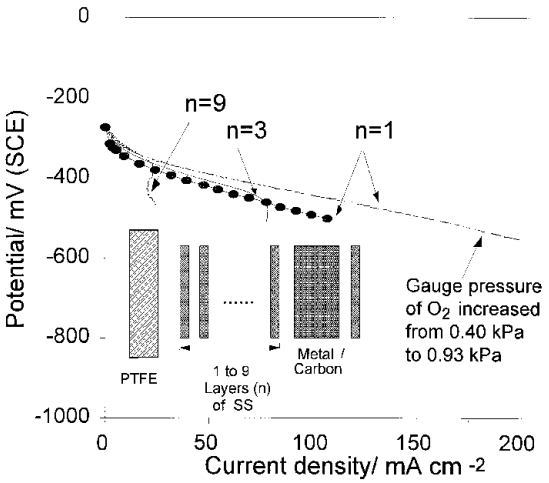

Fig. 11. Effect of stainless steel overlayers placed at the gas side of the electrode. Also shown is the effect of oxygen overpressure.

effectively those carbon fibres located close to the Teflon separator.

Figure 11 also demonstrates that the critical reaction zone can be brought even closer to the gas plenum by increasing the oxygen gauge pressure. In the additional experiment, the oxygen gauge pressure was slowly increased from 0.40 to 0.93 kPa until incipient bubbling into the electrolyte occurred. In this condition, oxygen displaces larger macro-void space within the electrode and diminishes the liquid film thickness greatly, resulting in the lower mass transport resistance, which is further supported by the much reduced value of R ($0.87\,\Omega\,cm^2$) shown in Table 2.

3.8. *Comparisons with conventional electrodes*

Figure 12 is a comparison of polarization data obtained for the composite electrode (C3, total weight 16 $mg\,cm^{-2}$) and a Teflon bonded commercial electrode (Prototech, Inc., total weight 113 $mg\,cm^{-2}$ with 0.45 mg Pt cm^{-2}). Teflon-bonded electrodes usually exhibit varying performances according to the changes of wetting [18]. In this experiment, at

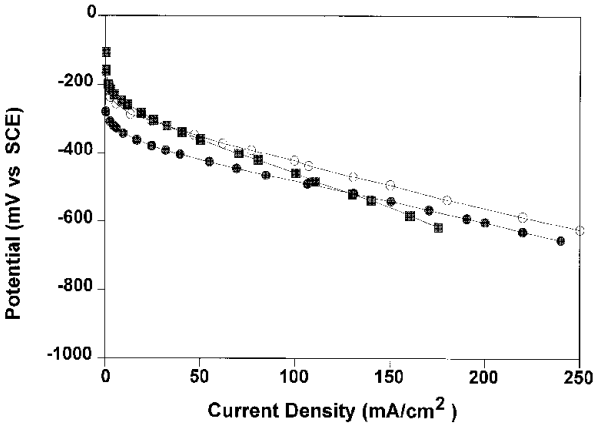

Fig. 12. Polarization curves for a metal–carbon composite electrode (C3, Table 1), a commercial Teflon-bonded electrode (i.e., Prototech) and a C3 with Pt. Key: (○) composite electrode with 12 wt % Pt; (■) commercial electrode (0.45 mg Pt cm^{-2}, 10 wt % on C); (●) composite electrode (no Pt).

the initial stage of operation, the Prototech electrode showed very poor performance due to extremely shallow penetration of electrolyte into the porous electrode structure [15]. However, the performance gradually increased during several polarization scans but began to degrade slowly due to electrode flooding. To make a comparison with the composite electrode, best three polarization curves were recorded prior to the onset of performance degradation. The data were averaged and reported in Fig. 12. At low current densities, the commercial electrode was superior due to the higher inherent electrochemical activity of Pt. The higher activity of Pt was also clear in terms of higher E_0 value, that is, −207 mV vs SCE. At higher current densities (> 120 mA cm^{-2}), however, the composite electrode showed less polarization losses even though the composite material did not contain Pt. The composite provided about seven times higher current per electrode weight than the commercial electrode at about −525 mV vs SCE (see Table 3 for a comparison of physical properties).

Also shown in Fig. 12 is a platinum-impregnated composite electrode, which was prepared from a preform sheet containing preplatinized carbon fibres (∼12 wt % Pt on carbon). The carbon fibres were impregnated with chloroplatinic acid using an incipient wetness technique and calcined before preparing the electrode preform. The average crystallite size of Pt was determined using hydrogen chemisorption and was 2.6 nm before sintering the preform and 18 nm after sintering. Obviously, the loss of surface area of the supported platinum was significant during the high temperature sintering, which necessitates incorporating platinum after sintering the electrode structure. Further work on this issue is now in progress. With platinum in the composite structure, the performance in the lower current density region was enhanced and approached that of the commercial electrode even though the surface area of platinum was lower in the composite electrode.

The combined resistance (ohmic and mass transport resistance) indicated by the slope of the polarization curve in the linear region was lower in the composite electrode than in the commercial electrode.

Table 3. Comparison of a composite electrode with a commercial electrode

	*Commercial**	*Composite (no Pt)*
Electrode weight/mg cm^{-2}	113	16
Thickness/mm	0.42	0.14
Cost/\$ cm^{-2}	1.5†	3.0×10^{-4} ‡
Current per electrode weight at −525 mV vs SCE/A g^{-1}	1.15	8.13

* Commercial electrode, Prototech, obtained from Electrosynthesis, Inc.
† Purchase price.
‡ Estimated from the material cost.

4. Conclusions

Electrode structures utilizing high aspect ratio fibrous precursors were fabricated in a novel process by entrapping a matrix of high surface area carbon fibres of about 2 μm diameter within a sinter-fused network of 2 μm diameter stainless steel fibres. The performances of various composite fibre electrodes were examined for oxygen reduction in a KOH half cell at room temperature. The effects of metal loading, carbon loading and electrode thickness were examined during polarization studies.

Within the composite electrode, there seems to exist a 'critical thickness region' close to the gas–liquid interface where mass transport is facile and catalyst loading and activity must be optimized at anticipated reaction conditions. Under current electrode operating conditions, this 'critical thickness' lies within the boundaries of an electrode containing about 3.5 mg carbon cm^{-2}, which is 0.14 mm thick. Preform pressing prior to sintering can be used to effectively concentrate carbon fibres within this thickness.

Significant reductions in polarization and mass transport resistances were observed by compacting the composite electrode structure so as to place more active electrocatalyst (i.e., carbon) in closer proximity to the gas source. Performance behaviour approached a maximum, however, when thickness/compaction levels were attained which reduced electrode void volume to such an extent that intraelectrode mass transport limitations were encountered. The rate limiting step in this process was determined to be the diffusion of oxygen, dissolved within the electrolyte, from the gas plenum through the interfibre macroporous channels of the electrode and into the interior of the electrode. Decreasing the thickness of the electrode structure placed more catalyst in closer proximity to the gas plenum, up to the point where the concomitant reduction in void volume provided a limitation in the intraelectrode void channels available for oxygen/electrolyte mass transport.

Compared to a commercial Teflon-bonded electrode, the composite electrode exhibits lower combined resistances and provides higher currents per electrode weight and volume. In the composite structure, sintered-metal fibre networks provide a highly conductive three-dimensional current collecting medium as well as a structural support to the active carbon within the electrode. The dual functionality reduces electrode weight and is more efficient than other forms of current collectors such as perforated metal foils or wire screens and meshes. With these attributes and high macroporosity, the composite electrodes appear as a suitable candidate for applications in various air electrodes among others.

Acknowledgement

This work was sponsored by the Army Research Office through University Research Initiative under grant DAAL03-92-G-0205.

References

[1] A. J. Appleby and F. R. Foulkes, 'Fuel Cell Handbook', Van Nostrand Reinhold, New York (1989) p. 357.

[2] E. L. Littauer and J. F. Cooper, *in* 'Handbook of Batteries and Fuel Cells' (edited by D. Linden), McGraw-Hill, New York (1984) pp. 30–1.

[3] M. R. Tarasevich and E. I. Khrushcheva, *in* 'Modern Aspects of Electrochemistry' (edited by B. E. Conway, J. O'M Bockris and R. E. White), No. 19, Plenum Press, New York (1989) p. 295.

[4] A. J. Bard and L. R. Faulkner, 'Electrochemical Methods; Fundamentals and Applications', John Wiley & Sons, New York (1980) Chap. 3.

[5] K. Kinoshita, 'Carbon: Electrochemical and Physicochemical Properties', John Wiley & Sons, New York (1988) Chap. 5.

[6] D. A. Kohler, J. N. Zabasajja, A. Krishnagopalan and B. J. Tatarchuk, *J. Electrochem. Soc.* **137** (1990) 136.

[7] D. A. Kohler, J. N. Zabasajja, F. Rose and B. J. Tatarchuk, *ibid.* **137** (1990) 1750.

[8] B. J. Tatarchuk, M. F. Rose, A. Krishnagopolan and D. A. Kohler, *US Patent 5 080 963* (1992).

[9] B. J. Tatarchuk, *US Patent 5 096 663* (1992).

[10] B. J. Tatarchuk, M. F. Rose and A. Krishnagopolan, *US Patent 5 102 745* (1992).

[11] J. O'M. Bockris and S. Srinivasan, 'Fuel Cells: Their Electrochemistry', McGraw-Hill, New York (1969) Chap. 8.

[12] S. F. Bender and J. W. Cretzmeyer, *in* 'Handbook of Batteries and Fuel Cells', *op. cit.*, pp. 7–10.

[13] R. J. Brodd, *in* 'Handbook of Batteries and Fuel Cells', *op. cit.*, pp. 17–20.

[14] S. Ahn, PhD dissertation, Auburn University, DCN.A452 (1992).

[15] S. Ahn and B. J. Tatarchuk, *J. Electrochem. Soc.* **142** (1995) 4169.

[16] K. J. Vetter, 'Electrochemical Kinetics', Academic Press, New York (1967).

[17] Y. Rho, O. Velev, S. Srinivasan and Y. Kho, *J. Electrochem. Soc.* **141** (1994) 2084.

[18] R. Holze and W. Vielstich, *Electrochim. Acta* **29** (1984) 607.